Proceedings of the
4th JSME-KSME Thermal Engineering Conference
October 1-6, 2000, Kobe, Japan

F307

CONTROL OF WALL SHEAR TURBULENCE WITH ARRAYED MICRO SENSOR/ACTUATOR UNITS

Takahide Endo*1, Nobuhide Kasagi, and Yuji Suzuki

Department of Mechanical Engineering, The University of Tokyo,
Hongo 7-3-1, Bunkyo-ku, Tokyo, 113-8656, Japan

ABSTRACT

Direct numerical simulation of turbulent channel flow was made in order to evaluate the feedback control with distributed micro sensor/deformable actuator units. The authors have developed a new realizable algorithm to detect quasi-streamwise vortices near the wall by only using the information of wall shear stresses [1]. In the present study, this control algorithm is applied to the drag reduction of the turbulent channel flow. Contrary to the previous studies of turbulence control, each deformable actuator is assumed to have finite dimensions. By the present control scheme with the arrayed sensor/actuator units, 17% drag reduction is achieved through selective manipulation of the streamwise vortices. It is found that the deformation of the actuators directly attenuate the streamwise vortices. When the streamwise vortices are diminished, the meandering of the streak becomes inactive, and the regeneration cycle of the streamwise vortices is attenuated.

Key Words: Wall Flow, Turbulence Control, Micro Actuators, DNS

1. INTRODUCTION

Turbulence and concomitant phenomena such as heat transfer, mass diffusion, friction drag and noise play important roles in industrial and environmental problems. From the view point of saving power and protecting the environment, it is strongly desired to develop efficient turbulence control techniques for momentum and heat transfer. Among various methodologies, active feedback control attracts much attention because of its large control effect with small control input [2-4].

Since the 1960's, a considerable degree of knowledge has been accumulated on the turbulent coherent structures and their underlying mechanism (e.g., [5]). Among those coherent structures, quasi-streamwise vortices (QSV; hereafter) are known to play a dominant role in the near-wall turbulent transport phenomena [6,7]. Jeong *et al.* [8] showed that QSV tilted in the spanwise direction has close relation with the meandering of low-speed streaks, and makes major contribution to the regeneration mechanism. Kravchenko *et al.* [9] showed that the streamwise vorticity accompanied with QSV has strong correlation with the wall shear stress upstream of the QSV. Kasagi & Ohtsubo [10] found that the production and destruction of the Reynolds shear stress as well as the turbulent heat flux are concentrated in the regions close to QSV. These facts indicate that an effective control of friction drag and/or heat transfer in wall turbulence can be established through selective manipulation of QSV.

Choi *et al.* [11] investigated turbulent channel flow with local blowing/suction on the wall, which is opposite to the wall-normal velocity in the buffer layer. They obtained 30% drag reduction in their direct numerical simulation (DNS; hereafter), and found that QSV are attenuated. Bewley *et al.* [12] employed a suboptimal control theory [13] in order to determine the distribution of wall blowing/suction as control input. They obtained 15% drag reduction and showed that the spatial distribution of blowing/suction determined by their suboptimal scheme is similar to that of Choi *et al.* [11].

Lee *et al.* [14] have developed a control algorithm based on neural networks. They determined the control input by using only wall variables, and found that the wall shear is substantially decreased when the blowing/suction rate is roughly proportional to the spanwise gradient of the spanwise shear stress.

It is noted that, in most previous DNS studies for controlling wall turbulence, an infinite number of sensors and actuators were assumed, and their volumes were neglected. Since these assumptions are unrealistic, it is desired to develop a new control algorithm assuming arrayed sensors and actuators of finite spatial dimensions.

Devices for turbulence feedback control should have

*1 Present address: Computer and Information Division, The Institute of Physical and Chemical Research (RIKEN), Hirosawa 2-1, Wakou-si, Saitama, 351-0198, Japan.
E-mail: tendo@postman.riken.go.jp

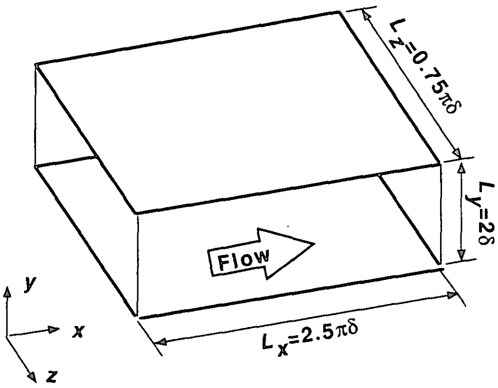

Figure 1. Flow geometry and coordinate system.

spatio-temporal scales comparable with those of the coherent structures [15]. Recent development of micro-electromechanical systems (MEMS) technology enables us to fabricate prototypes of such micro devices [16]. Among various kinds of actuators, wall deformation is considered to be one of the most promising candidates, because of its robustness against the hostile environment [17].

Endo *et al.* [1] employed DNS of turbulent channel flow with actively deformed walls. They showed that about 12% drag reduction is observed when the wall velocity is given so as to be out-of-phase of the wall-normal velocity in the buffer region. The power input for deforming walls are fairly small than the pumping power saved, and it is shown that the wall deformation is effective in turbulence control. They also found the characteristic dimensions of effective wall deformation, i.e., about 200 and 60 viscous length units in the streamwise and spanwise directions, respectively.

They have developed a new algorithm to detect QSV near the wall from the wall shear stresses in their DNS of turbulent channel flow with arrayed sensor/deformable actuator units on the walls. They showed that QSV is successfully captured by the spanwise gradients of wall shear stress, and that QSV is observed at 50 ν/u_τ downstream from the sensing location. The friction drag is reduced as much as 17%, although the sensors and actuators are distributed rather coarsely.

The objective of the present study is to investigate the the drag reduction mechanism under the control with arrayed sensor/deformable actuator units.

2. NUMERICAL PROCEDURE

The flow geometry and the coordinate system are shown in Fig. 1. The governing equations are the incompressive Navier-Stokes equations and the continuity equation. The wall deformation is represented by a boundary-fitted coordinate system for moving boundary. Periodic boundary conditions are employed in the streamwise ($x-$) and spanwise ($z-$) directions, while non-slip boundary condition is imposed on the top and bottom deformable walls.

A modified Crank-Nicolson type fractional-step method [18] is used for the time advancement, while a second-order finite difference scheme is employed for the spatial discretization of both flow variables and metrics on a staggered mesh [19].

The size of the computational volume is respectively $2.5\pi\delta$ and $0.75\pi\delta$ in the $x-$ and $z-$ directions, where δ is the channel half width. The simulation is performed under a constant flow rate condition throughout the present study. The Reynolds number based on the bulk mean velocity U_b and the channel width 2δ is 4600 (about 150 based on the wall friction velocity u_τ and δ). The computational domain is about 1180 and 360 viscous length scales in the $x-$ and $z-$ directions, respectively. Hereafter, $(\ )^+$ represents a quantity non-dimensionalized by the friction velocity u_τ in the plane channel flow without control and the kinematic viscosity ν.

The number of grid points is 96, 97 and 96 in the $x-, y-$ and $z-$directions, respectively. A non-uniform mesh with a hyperbolic tangent distribution is employed in the $y-$direction. The first mesh point away from the wall is given at $y^+ = 0.25$. The computational time step is chosen as $0.33\nu/u_\tau^2$. The initial condition is given from a fully-developed velocity field of preceding channel flow DNS.

3. DETECTION OF QUASI-STREAMWISE VORTEX BASED ON WALL VARIABLES

It is well known that the near-wall streaky structures do not always flow straight in the streamwise direction, but often meander in the spanwise direction. Hamilton *et al.* [20] pointed out that QSV and the streaky structure have close dynamical relationship with each other, and the meandering of streaks plays an important role in a quasi-cyclic process of turbulence regeneration. Jeong *et al.* [8] proposed a schematic model of QSV alternatively tilting in the $x-z$ plane associated with the meandering of the near-wall low-speed streak. From the information mentioned above, it is expected that QSV can be identified by detecting the streak meandering.

Figure 2 shows a schematic of a modelled streaky structure. When the velocity gradients in the two horizontal directions are taken into account, the edges of the streak can be grouped into four events E1~E4, depending on the signs of $\partial u'/\partial x$ and $\partial u'/\partial z$. Note that E1 and E4, and also E2 and E3 are respectively of mirror symmetry in the spanwise direction.

Endo *et al.* [1] investigated a conditionally averaged flow field around the meandering streaks given the condition of the combination of the signs $\partial u'/\partial x$ and $\partial u'/\partial z$ at $y^+ = 15$ using DNS database of turbulent channel flow. They showed that the QSV with strong streamwise vortices are observed at the downstream edge of low-speed streaks, i.e.; large peaks of positive and negative ω_x are observed at Events E1 and E4, respectively, while negligible values of ω_x are observed at Events E2

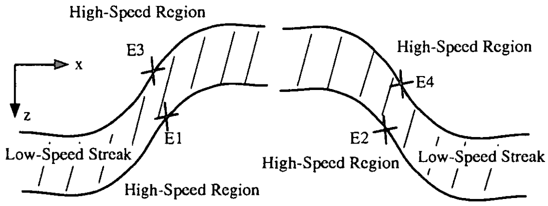

Figure 2. Schematic of a modelled streaky structure.

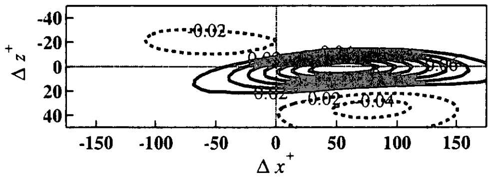

Figure 3. Contours of streamwise vorticity at $y^+ = 15$, given the conditions of $\partial \tau_u^+ / \partial z^+ > 0.035$ and $\partial \tau_w^+ / \partial z^+ < -0.005$.

and E3.

They also showed that the spanwise gradients of τ_u^+ ($\equiv \partial u'^+ / \partial y^+|_w$) and τ_w^+ ($\equiv \partial w'^+ / \partial y^+|_w$) instead of the velocity gradients in the buffer layer are good indicators for the meandering streaks. The signs of the shear stress gradients and the corresponding events are summarized in Table 1. A negative value of $\partial \tau_w / \partial z$ is observed $50\nu/u_\tau$ upstream of Events E1 and E4, while $\partial \tau_w / \partial z > 0$ for E2 and E3. Note that Event E1 can be distinguished from E4 by the sign of $\partial \tau_u / \partial z$ at the same location.

Figure 3 shows the contours of the streamwise vorticity $< \omega_x^+ >$ at $y^+ = 15$, conditionally averaged for S1 ($\partial \tau_u^+ / \partial z^+ > 0.035$ and $\partial \tau_w^+ / \partial z^+ < -0.005$). A large peak of streamwise vorticity is well captured at $50\nu/u_\tau$ downstream from the detection point. Although it is not shown here, a large negative peak of ω_x^+ is associated with S4 ($\partial \tau_u^+ / \partial z^+ < -0.035$ and $\partial \tau_w^+ / \partial z^+ < -0.005$), which corresponds to Event E4. Thus, QSV as well as its direction of rotation can be detected by the combination of the signs of shear stress gradients, i.e.; $\partial \tau_u^+ / \partial z^+$ and $\partial \tau_w^+ / \partial z^+$.

Figure 4 shows contours of the conditionally averaged wall-normal velocity $< v'^+ >$ at $y^+ = 15$ for S1. Positive and negative peaks are aligned side-by-side in the spanwise direction, and they respectively correspond to the ejection and sweep motions. The spanwise distance of the positive and negative peaks is about $30\nu/u_\tau$, which is almost the same as the mean diameter of QSV [6].

4. FEEDBACK CONTROL WITH ARRAYED DEFORMABLE ACTUATORS

In previous studies, sensors and actuators are assumed to be infinitely small, and placed at each computational grid point on the wall. In the present study, we assume control devices having finite dimensions, and design arrayed actuators and sensors based on the discussion described above.

Table 1. Four signals and corresponding events.

Signal	$\partial \tau_u / \partial z$	$\partial \tau_w / \partial z$	Event	ω_x'
S1	Positive	Negative	E1	Positive
S2	Positive	Positive	E2	
S3	Negative	Positive	E3	
S4	Negative	Negative	E4	Negative

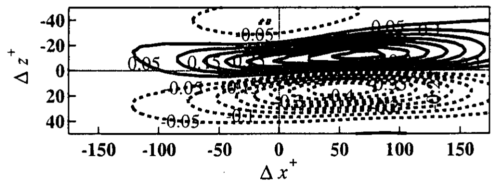

Figure 4. Contours of wall-normal velocity at $y^+ = 15$, given the conditions of $\partial \tau_u^+ / \partial z^+ > 0.035$ and $\partial \tau_w^+ / \partial z^+ < -0.005$.

Figure 5 (a) shows a schematic of deformable actuator assumed in the present study. By taking into account the characteristic length of the wall deformation [1], the streamwise and spanwise dimensions of the actuator is chosen as 172 and $60\nu/u_\tau$, respectively. Each actuator is assumed to be deformed only in the $y-$direction. The shape is determined with a sinusoid in the spanwise direction, in such a way that the distance between the peak and trough is about the mean diameter of QSV.

Figure 5 (b) shows an arrangement of arrayed shear stress sensors and deformable actuators. A shear stress sensor is assumed to be centered at $12.3\nu/u_\tau$ upstream from the upstream end of the deformable actuator. Hence, the streamwise distance between the sensor and the center of the actuator is $50\nu/u_\tau$, which corresponds to the displacement between the detection point of Events E1 and E4, and the peak of the streamwise vorticity shown in Fig. 4. In the present study, 36 sensor/actuator units (6 × 6 in the streamwise and spanwise directions) are distributed with a regular pitch on both walls of the channel.

Each sensor measures the spanwise gradients of the instantaneous wall shear stresses, $\partial \tau_u / \partial z$ and $\partial \tau_w / \partial z$. The wall velocity at the center of the peak/trough of the actuator v_m is determined by:

$$v_m^+(t_{n+1}) = \begin{cases} \alpha \tanh\left(\dfrac{\partial \tau_u^+(t_n)}{\partial z^+}/\beta\right) - \gamma y_m^+(t_n), & \\ \qquad \text{if } \dfrac{\partial \tau_w(t_n)}{\partial z} < 0, & \\ -\gamma y_m^+(t_n), \quad \text{otherwise}, & \end{cases} \tag{1}$$

where y_m is the wall displacement at the peak/trough, and α, β, and γ are control parameters, respectively. The wall velocity of each grid point on the actuator is given by

$$v_w^+(t_{n+1}) = v_m^+(t_{n+1}) \cdot f(x^+) \cdot \exp\left[-\frac{(z^+ - z_c^+)^2}{\sigma_z^{+2}}\right] \cdot \sin\left[\frac{2\pi(z^+ - z_c^+)}{m_z^+}\right], \tag{2}$$

(a)

(b)

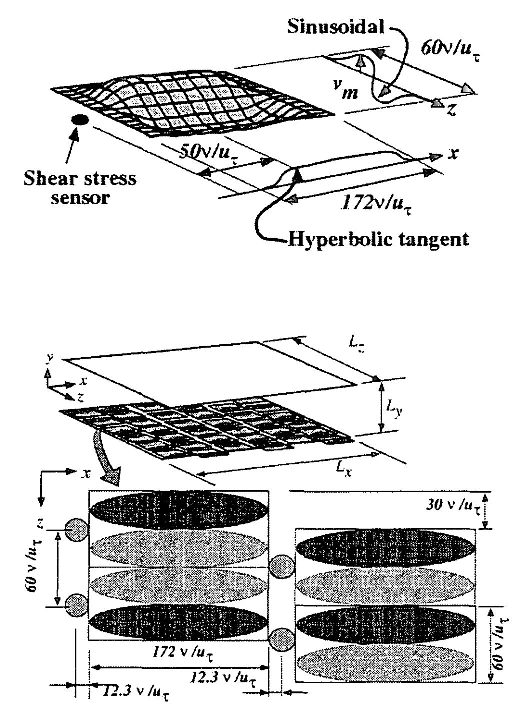

Figure 5. Schematic of arrayed actuators and shear stress sensors. (a) Dimension of a single deformable actuator. (b) Arrangement of the actuators and the sensors.

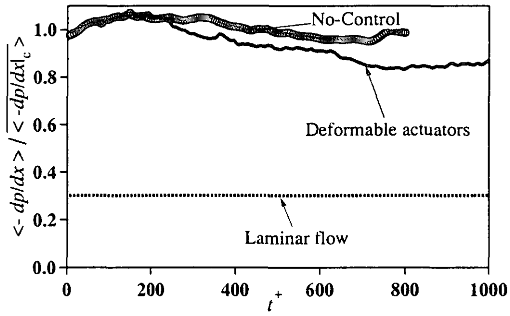

Figure 6. Time trace of the normalized mean pressure gradient.

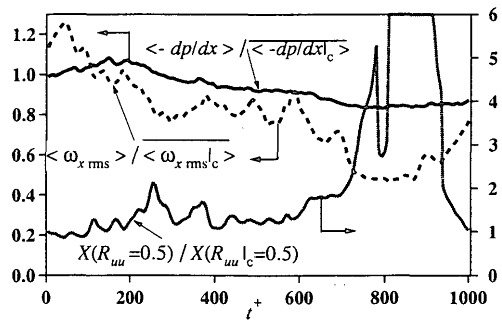

Figure 7. Time trace of the normalized mean pressure gradient, streamwise vorticity and two-point correlation of streamwise velocity fluctuation.

where the function $f(x^+)$ is introduced to keep the shape of the actuator smooth in the streamwise direction. The function f is determined with a hyperbolic tangent as:

$$f(x^+) = \begin{cases} \frac{1}{2}\left[1+\tanh\left\{\frac{(x^+-x_c^+)+73.7}{\sigma_x^+}\right\}\right] \\ \qquad \cdots \text{if } -86 \le x^+ - x_c^+ \le -61.5, \\ 1 \qquad \cdots \text{if } -61.5 \le x^+ - x_c^+ \le 61.5, \\ \frac{1}{2}\left[1-\tanh\left\{\frac{(x^+-x_c^+)-73.7}{\sigma_x^+}\right\}\right] \\ \qquad \cdots \text{if } 61.5 \le x^+ - x_c^+ \le 86. \end{cases} \tag{3}$$

In Eqs. (2) and (3), x_c and z_c denote the location of the center of the actuator. The parameters are somewhat tuned through preliminary computations, and chosen as $\alpha = 2.3, \beta = 0.077, \gamma = 0.3, \sigma_x^+ = 6.14$, and $\sigma_z^+ = 22.2$, respectively.

Figure 6 shows a time trace of the mean pressure gradient normalized by that without control. The present result, however, exhibits no control effect until $t^+ = 200$, and then the drag is decreased at $t^+ > 200$. A maximum drag reduction rate of 17% is obtained at $t^+ = 800$. Therefore, even with coarsely distributed sensors and actuators on the wall, the present control scheme appears to be efficient through selective manipulation of QSV. It is expected that the time lag for appearing the control effect is caused by the spatial phase relation of QSV and coarsely distributed sensors. Although it is not shown here, the energy input for deforming actuators are much smaller than the pumping power saved.

Figure 7 shows a time trace of the normalized streamwise vorticity at $y^+ = 15$, with mean pressure gradient under the present control. The streamwise vorticity is diminished relatively faster than the pressure gradient by the control. From this, it is expected that the deformable actuator which has a sinusoidal shape in the spanwise direction, directly attenuates the rotation of the QSV. As a result, the friction drag is reduced.

Temporal evolution of the two-point correlation of the velocity fluctuations are computed from the instantaneous field. In Fig. 7, time trace of the characteristic streamwise distance $X(R_u u = 0.5)$ in which the streamwise two-point correlation of the streamwise component is decreased to 0.5. The quantity is normalized by that without control. As the drag is decreased, $X(R_u u = 0.5)$ is increased. It is conjectured that the increase in the streamwise two-point correlation is due to the reduction of the streak meandering. By comparing the time traces shown in Fig. 7, the streamwise vorticity fluctuation is decreased as soon as the onset of the control, followed by the decrease in drag and the increase in the two-point correlation.

Figure 8 shows the top views of instantaneous flow fields at $t^+ = 0$ and 604. Vortical structures are identified with their negative value of the second invariant of the deformation tensor ($II' = u'_{i,j}u'_{j,i}$) [21],[7]. Before the present control is adopted, the low-speed streaks meander in the spanwise direction, and the vortical structures are active and regenerated continuously. However, QSV becomes less populated near the wall under the present control as shown in Fig. 8(b). Meandering of

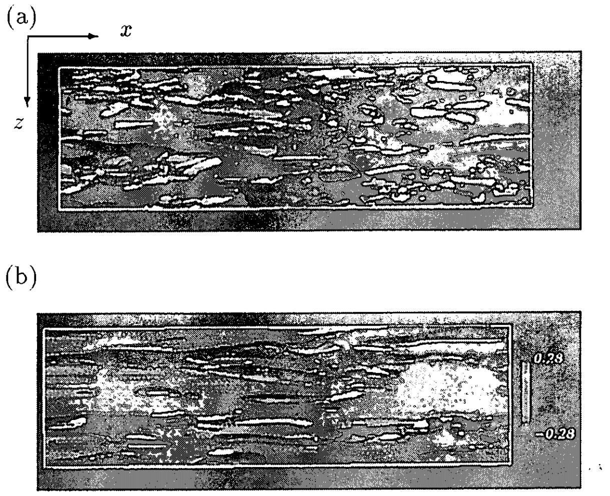

Figure 8. Top view of the instantaneous flow field. Flow: left to right. White: $II'^{+} = -0.03$, Dark grey: $u'^{+} = -3.5$, Light grey: $u'^{+} = 3.5$. (a) $t^{+} = 0$, (b) $t^{+} = 604$.

the low-speed streaks becomes inactive and longer in the streamwise direction. As it is discussed in Fig. 7, two-point correlation of u' in the streamwise direction shows higher values under the control than that without control.

Figure 9 shows the rms values of vorticity fluctuations. Since the wall has finite wall-normal velocity component, it produces higher ω_x at the wall, although all components of vorticity fluctuations are diminished near the wall.

The evolution equation of ω_x is written as:

$$\frac{D\omega_x}{Dt} = \omega_x \frac{\partial u}{\partial x} + \omega_y \frac{\partial u}{\partial y} + \omega_z \frac{\partial u}{\partial z} + \nabla^2 \omega_x. \tag{4}$$

The terms on the RHS of Eq. (4) are the production term due to stretching, tilting, twisting, and viscous diffusion, respectively. The largest term in the RHS in Eq. (4) is $(\partial u/\partial z)(\partial u/\partial y)$, which is involved in tilting and twisting terms with alternative signs, so that it has no net contribution [22]. Therefore, it is convenient to rewrite Eq (4) as:

$$\frac{D\omega_x}{Dt} = \omega_x \frac{\partial u}{\partial x} - \left(\frac{\partial w}{\partial x}\right)\left(\frac{\partial u}{\partial y}\right) + \left(\frac{\partial v}{\partial x}\right)\left(\frac{\partial u}{\partial z}\right) + \nabla^2 \omega_x. \tag{5}$$

Since the stretching term is zero where the streamwise vorticity does not exist, the streamwise vorticity is mostly generated by the tilting term in its early stage. Once the streamwise vorticity is formed, it is strengthened by the stretching term. The tilting term as well as the stretching term has close relation with the streak meandering, since both terms have spatial gradient of velocity field. Thus it is expected that all production terms are suppressed under the present control by diminishing the meandering of the streak.

Figure 10 shows the rms value of the production terms in Eq. (5). Although the stretching term and the term derived from tilting term has non-zero value at the wall,

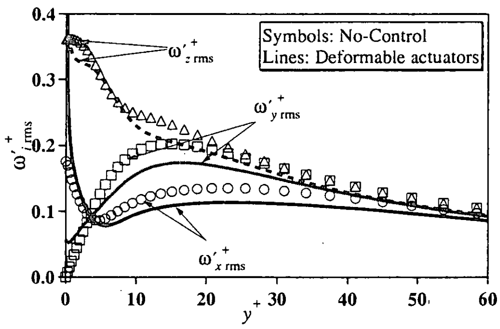

Figure 9. RMS value of vorticity fluctuation.

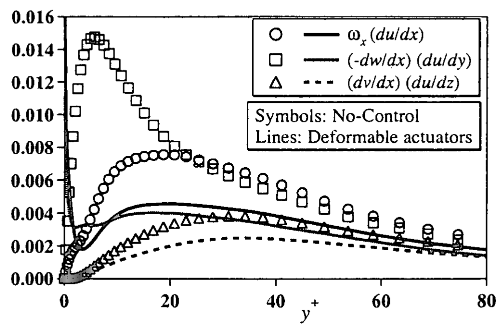

Figure 10. Production terms of streamwise vorticity.

all production terms are successfully suppressed near the wall by the present control.

Figure 11 shows an instantaneous spatial distribution of strong stretching of QSV. The threshold of $|\omega_x^{+} \cdot (\partial u'^{+}/\partial x^{+})| = 0.01$ is used to extract strong stretching. The stretching is actively induced at the edge of the meandering low-speed streaks. When the meandering of the streak is suppressed by the present control, the stretching is diminished. Although it is not shown here, the tilting is also weakened by the present control.

From these observations, it is expected that meandering of the streaks is inactivated by diminishing the rotation of the QSV, using the arrayed deformable actuators. When the meandering of the streaks becomes mild, it leads to a calm spatial gradient of the velocity fluctuation. Hence, production of streamwise vorticity becomes small. As a result, regeneration of the QSV is attenuated and friction drag reduced. This control mechanism is schematically illustrated in Fig. 12.

5. CONCLUSIONS

A simple control scheme using only wall variables is achieved with arrayed sensor/deformable actuator units in the direct numerical simulation of turbulent channel flow and 15% drag reduction is achieved. This fact shows a realizable control is expected through selective manipulation of QSV, although micro sensors/actuators are distributed rather coarsely on the wall.

The rotation of the streamwise vortices is directly attenuated by distributed deformable actuators which has

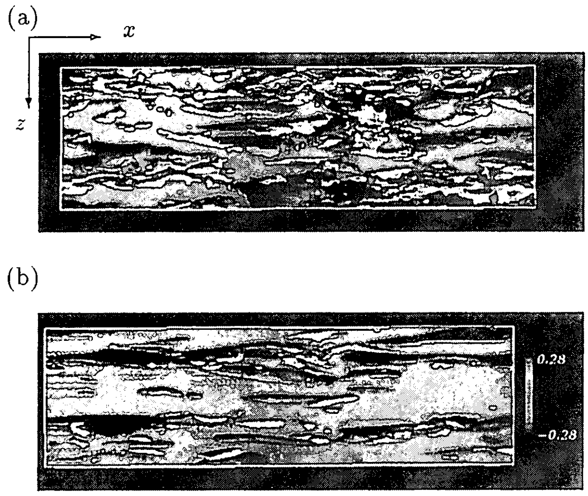

Figure 11. Top view of the instantaneous flow field. Flow: left to right. White: $|\omega_x^+ \cdot (\partial u'^+/\partial x^+)| = 0.01$, Dark grey: $u'^+ = -3.5$, Light grey: $u'^+ = 3.5$. (a) $t^+ = 0$, (b) $t^+ = 604$.

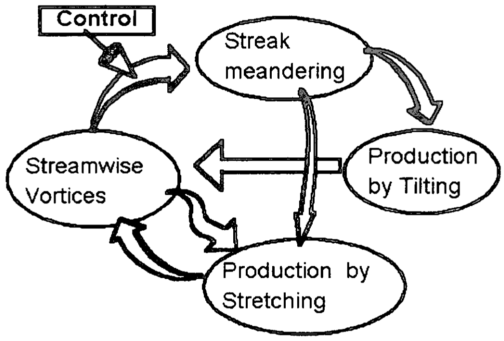

Figure 12. Schematic illustration of regeneration of streamwise vortices and the control mechanism.

sinusoidal shape in spanwise direction. The meandering of streak is suppressed by small streamwise vorticity, and the regeneration of the streamwise vortex is diminished. As a result, the generation cycle of the streamwise vortices is cut off, and then, drag reduction is obtained.

REFERENCES

[1]Endo, T., Kasagi, N., and Suzuki, Y., 1999, "Feedback Control of Wall Turbulence with Wall Deformation," 1st Int. Symp. Turbulence & Shear Flow Phenomena, Santa Barbara, pp. 405-410.

[2] Moin, P., and Bewley, T., 1994, "Feedback control of turbulence," Appl. Mech. Rev., Vol. 47, S3-S13.

[3]Gad-el-Hak, M., 1996, "Modern developments in flow control," Appl. Mech. Rev., Vol. 49, pp. 365-377.

[4]Kasagi, N., 1998, "Progress in direct numerical simulation of turbulent transport and its control," Int. J. Heat & Fluid Flow, Vol. 19, pp. 125-134.

[5]Cantwell, B. J., 1981, "Organized motion in turbulent flow," Ann. Rev. Fluid Mech., Vol. 13, pp. 457-515.

[6]Robinson, S.K., 1991, "Coherent motions in the turbulent boundary layer," Annu. Rev. Fluid Mech., Vol. 23, pp. 601-639.

[7]Kasagi, N., Sumitani, Y., Suzuki, Y., and Iida, O., 1995, "Kinematics of the quasi-coherent vortical structure in near-wall turbulence," Int. J. Heat & Fluid Flow, Vol. 16, pp. 2-10.

[8]Jeong, J., Hussain, F., Schoppa, W., and Kim, J., 1997, "Coherent structures near the wall in a turbulent channel flow," J. Fluid Mech., Vol. 332, pp. 185-214.

[9]Kravchenko, A. G., Choi, H., and Moin, P., 1993, "On the relation of near-wall streamwise vortices to wall skin friction in turbulent boundary layers," Phys. Fluids A, Vol. 5, No. 12, pp. 3307-3309.

[10]Kasagi, N., and Ohtsubo, Y., 1992, "Direct numerical simulation of low Prandtl number thermal field in a turbulent channel flow," Turbulent Shear Flows 8, Durst *et al.* eds., Springer-Verlag, Berlin, pp. 97-119.

[11]Choi, H., Moin, P., and Kim, J., 1994, "Active turbulence control for drag reduction in wall-bounded flows," J. Fluid Mech., Vol. 262, pp. 75-110.

[12]Bewley, T.R., Choi, H., Temam R., and Moin P., 1993, "Optimal feedback control of turbulent channel flow," CTR Annual Research Briefs, Stanford Univ., pp. 3-14.

[13]Choi, H., Temam, R., Moin, P., & Kim, J., 1993, "Feedback control for unsteady flow and its application to the stochastic Burgers equation," J. Fluid Mech., Vol. 253, pp. 509-543.

[14]Lee, C., Kim, J., Babcock, B., and Goodman, R., 1997, "Application of neural networks to turbulence control for drag reduction," Phys. Fluids, Vol. 9, pp. 1740-1747.

[15]Gad-el-Hak, M., 1994, "Interactive Control of Turbulent Boundary Layers: A Futuristic Overview," AIAA J., Vol. 32, No. 9, pp. 1753-1765.

[16]Ho, C-M., and Tai, Y-C., 1996, "Review: MEMS and Its Applications for Flow Control," ASME J. Fluids Eng., Vol. 118, pp. 437-447.

[17]Grosjean, C., Lee, G. B., Hong, W., Tai, Y.-C., and Ho, C.-M., 1998, "Micro Balloon Actuators for Aerodynamic Control," Proc. 11th MEMS Workshop, pp. 166-171.

[18]Choi, H., and Moin, P., 1994, "Effects of the computational time step on numerical solutions of turbulent flow," J. Comput. Phys. Vol 113, pp. 1-4.

[19]Mito, Y., and Kasagi, N., 1998, "DNS study of turbulence modification with streamwise-uniform sinusoidal wall-oscillation," Int. J. Heat & Fluid Flow, Vol 19, pp. 470-481.

[20]Hamilton, J. M., Kim, J., and Waleffe, F., 1995, "Regeneration mechanism of near-wall turbulence structures," J. Fluid Mech., Vol. 287, pp. 317-348.

[21]Chong, M. S., Perry, A. E., & Cantwell, B. J., 1990, "A general classification of three dimensional flow fields," Phys. Fluids A, Vol. 2, No. 5, pp. 765-777.

[22]Brooke, J. W., & Hanratty, T. J., 1993, "Origin of the turbulence-producing eddies in a channel flow," Phys. Fluids A, Vol. 5, No. 4, pp. 1001-1022.